Effects of microstructure on crack tip fields and fracture toughness in PC/ABS polymer blends

Seelig, Thomas; Van der Giessen, Erik

Published in:
International Journal of Fracture

DOI:
10.1007/s10704-007-9117-y

Publication date:
2007

Int J Fract (2007) 145:205–222
DOI 10.1007/s10704-007-9117-y

ORIGINAL PAPER

Effects of microstructure on crack tip fields and fracture toughness in PC/ABS polymer blends

Thomas Seelig · Erik Van der Giessen

Received: 22 March 2007 / Accepted: 23 August 2007 / Published online: 14 September 2007

Abstract Numerical simulations are performed in order to gain a better understanding of the effects of various microstructural features and toughening mechanisms in amorphous PC/ABS polymer blends. Crack tip loading under global small-scale yielding conditions is considered with the blend microstructure explicitly resolved in the near-tip process zone. Constitutive models are employed which account for large viscoplastic deformations, the characteristic softening-rehardening behavior of glassy polymers, as well as the effect of plastic dilatancy in the ABS phase due to rubber particle cavitation. The influence of blend composition and morphology on the local stress distribution and the development of the plastic zone at a stationary crack tip are analyzed. Furthermore, crack propagation and the evolution of fracture toughness are studied using different cohesive surface models for failure in the different phases of the blend microstructure.

Keywords Polymer blends · Microstructure · Crack tip fields · Toughening mechanisms · Crack resistance curves

T. Seelig (✉)
Fraunhofer-Institute for Mechanics of Materials,
Woehlerstrasse 11, Freiburg, 79108, Germany
e-mail: see@iwm.fhg.de

E. Van der Giessen
Materials Science Center, University of Groningen,
Groningen, 9747 AG, The Netherlands

1 Introduction

Polymeric materials used in technical applications are frequently composed of different constituents in order to improve their mechanical performance and other physical properties. An important class of materials which has received increasing attention in recent years are blends of polycarbonate (PC), an amorphous glassy thermoplastic, and acrylonitrile-butadiene-styrene (ABS). Since ABS itself is a two-phase material with small (butadiene) rubber particles dispersed in a matrix of styrene-acrylonitrile (SAN, also an amorphous glassy thermoplastic) PC/ABS is referred to as a *ternary* blend. Among several other reasons (e.g. better processability), one purpose of blending PC with ABS is to reduce the severe notch-sensitivity of neat PC and to increase the fracture toughness. Roughly speaking, this works because ABS is already a so-called rubber-toughened polymer where the dispersed rubber particles serve to initiate energy dissipating microscopic deformation mechanisms at many sites throughout the material. As an example of the toughening that can be achieved this way, Kinloch and Young (1983) report an impact fracture energy of sharply notched PC specimens which is only about 8% of the value for bluntly notched specimens while for ABS the respective value for sharply notched specimens is still about 60% of that for a blunt notch. In ABS as well as other "classical" rubber-toughened materials, such as high-impact polystyrene (HIPS), the beneficial role of the modifier phase in the intrinsically brittle glassy matrix is fairly well

understood (Bucknall 1977). PC, in contrast, displays an ambivalent behavior ranging from high ductility under unnotched conditions to brittle failure in the presence of a sharp notch. Hence, it is far less clear under which circumstances blends of PC and ABS show an improved mechanical performance. Another complicating factor is the enriched microstructure of PC/ABS with the ABS content in the blend, the morphology, and the rubber content in the ABS being the most important parameters from a mechanical point of view.

Despite the complex interrelation between these parameters some qualitative understanding of their effect on the macroscopic deformation and failure behavior of PC/ABS blends has emerged from a large number of experimental studies; see e.g. Greco (1996) for a review. A general trend reported in the experimental literature is that under tensile loading of unnotched specimens the ductility (strain at failure) of PC/ABS decreases with increasing ABS content because the ability of neat PC to undergo large strains and ductile neck propagation ("cold drawing") is hampered by the presence of the ABS (e.g., Greco et al. 1994; Balakrishnan and Neelakantan 1998). The dependence of the elastic stiffness and the yield stress of PC/ABS on the ABS content is controlled by the amount of (soft) rubber in the ABS since the SAN matrix of the latter is stiffer and has a higher yield stress than PC (e.g., Kurauchi and Ohta 1984; Greco et al. 1994; Ishikawa 1995). These dependencies can qualitatively be explained from simple rules of mixtures or other micromechanical considerations (Seelig 2004).

Far more complex, however, is the fracture behavior of PC/ABS blends as observed e.g., in Charpy impact or SENT tensile tests, and expressed in terms of fracture energies or crack resistance curves. For instance, Greco et al. (1994) found a pronounced synergistic effect, i.e., a fracture toughness of PC/ABS significantly higher than that of each constituent, for an intermediate range of 10–40% ABS in the blend, while this toughening effect in turn strongly depends on the ABS type. The latter was mainly determined by the rubber content, and the maximum toughness was observed at around 15% rubber in the ABS. Similar highly non-monotonous variations of the fracture properties with composition are reported by other researchers (e.g., Lee et al. 1992; Balakrishnan and Neelakantan 1998; Inberg 2001). In accordance with the above mentioned behavior of PC/ABS under unnotched conditions, an enhanced fracture toughness compared to that of neat PC is only observed for sufficiently sharp notches. In this situation neat PC typically fails by the formation and unlimited propagation of a single craze initiated by the concentration of hydrostatic stress ahead of the notch (e.g. Narisawa and Yee 1993). In contrast, the presence of ABS which is able to undergo volumetric expansion upon cavitation of the rubber particles causes a relief of hydrostatic stress (thereby suppressing crazing) and enables shear yielding in the PC. The qualitative picture of this toughening mechanism in PC/ABS, which is confirmed by microplastic deformations visible on the fracture surface, is generally agreed upon (e.g., Ishikawa and Chiba 1990; Lee et al. 1992; Seidler and Grellmann 1993; Greco et al. 1994; Ishikawa 1995; Inberg 2001). However, the efficiency of toughening strongly depends on various parameters, the rubber content in the ABS probably being the most important one. Another influence arises from the blend morphology which changes from one with ABS particles (of a few microns diameter) embedded in the PC matrix at low ABS content to a co-continuous (often lamellar) one when the ABS content is increased above 40% (Greco 1996; Inberg 2001). Obviously, the patterns of local plastic deformation (shear yielding) enabled in the PC—and perhaps so the efficiency of toughening—depend on this morphology. While the individual roles of these microstructural features in the toughening process can hardly be analyzed from experiments, it is the aim of the present work to gain some additional insight and basic understanding from micromechanical models and numerical simulations.

Mechanical modeling of rubber-toughened polymers is still in a rather early stage and so far has mostly focused on two-phase materials, i.e., a glassy matrix containing soft rubber particles, with the latter typically being treated as voids (Smit et al. 1999; Steenbrink and Van der Giessen 1999; Socrate and Boyce 2000; Pijnenburg and Van der Giessen 2001; Danielsson et al. 2002; Meijer and Govaert 2003). These studies have utilized cell models of the voided polymer subjected to uniform overall deformation in conjunction with a constitutive model for the deformation behavior of the glassy matrix, as the one developed by Boyce et al. (1988), and analyzed the effect of voids on matrix yielding and the reduction of hydrostatic stress as indicators of an enhanced toughness. Similarly, Seelig and Van der Giessen (2002) used cell models to investigate localized plastic deformations and stress distributions in ternary blends with ABS particles embedded

in a PC matrix. Cavitated rubber particles in ABS thereby were accounted for by describing ABS in a homogenized manner as a porous glassy polymer. Fracture mechanical models for a stationary crack tip have been applied to ABS materials by Pijnenburg et al. (2005), using a variety of ways to represent the microstructure under crack-tip loading conditions. In order to investigate the interaction of crack tip plasticity, crazing and subsequent crack propagation in homogeneous glassy polymers, Estevez et al. (2000) and Estevez and Van der Giessen (2005) employed a cohesive surface model of crazing as developed in (Tijssens et al. 2000).

As a natural continuation of the above approaches, the present work deals with crack tip fields, crack propagation and toughening mechanisms in PC/ABS blends. In Sect. 2 we start with an outline of how the blend microstructure is modeled in order to account for essential features of the different constituents. Also, the computational model for the blend material under crack tip loading conditions is described. Constitutive models for the finite strain deformation behavior of PC and ABS as well as for their failure—treated in the framework of a cohesive surface methodology—are presented in Sect. 3. These models involve a number of simplifying assumptions and hence the numerical results discussed in Sect. 4 are of a qualitative nature, but allow to investigate the separate effects of blend morphology and composition on the distribution of stress and plastic flow in the vicinity ('process zone') of a stationary crack tip. Afterwards, crack propagation is simulated and the influence of the ABS type (in terms of its rubber content) on the fracture toughness of the blend and its evolution in the course of crack advance is studied. As the present work is a first step in the numerical investigation of toughening mechanisms in PC/ABS blends, a critical discussion of the employed modeling concepts as well as suggestions for model improvements are given in Sect. 5.

2 Problem formulation

2.1 Blend modeling

The microstructure of a PC/ABS blend as shown by the micrograph in Fig. 1a consists of homogeneous regions of PC and regions of ABS which itself has a heterogeneous microstructure with rubber particles embedded in the SAN matrix. Due to loading of the material, the (dark) rubber particles visible in the micrograph have cavitated and grown to voids (bright). The morphology of the PC and ABS regions depends on their volume fractions and typical grades may contain up to 50% ABS. At a low ABS content (e.g., 30% and less) the ABS prevails as approximately spherical particles of a few microns diameter in the PC matrix whereas for 50/50 blends (micrograph in Fig. 1a) a co-continuous morphology (often lamellar due to injection moulding) is found with a thickness of the PC and ABS regions also of a few microns (Greco 1996; Inberg 2001).

In order to simplify the modeling of the microstructure of PC/ABS blends, the key assumption is made here that ABS can be described as a homogenized effective medium, so that the PC does not 'see' the individual rubber particles embedded in the SAN matrix of ABS (Fig. 1b). Moreover, since rubber particles cavitate at a relatively low stress level and have a stiffness much smaller than that of the surrounding glassy polymer, they are represented as voids in the present model (see also Sect. 3.2). Hence, PC/ABS ternary blends are described as a two-phase material consisting of a neat (PC) and a porous (ABS) glassy polymer. The same approach was adopted in (Seelig and Van der Giessen 2002) where details on the homogenization procedure may be found; a description of the resulting porous plasticity model for ABS is given in Sect. 3.2. Besides the enormous computational effort that would be needed to model the entire microstructure, the compromise of resolving only the PC and ABS regions by homogenizing the ABS is also motivated by the fact that in the present context we are interested in deformation mechanisms on the scale of the PC and ABS regions, e.g., shear banding in the PC enabled by the plastic dilatancy of the ABS under the highly triaxial overall loading as it prevails ahead of a crack tip.

2.2 Crack tip problem

As discussed in the Introduction an improved fracture toughness of PC/ABS blends compared to that of neat PC is observed only in case of a sufficiently sharp crack with a crack tip radius r_{tip} much smaller than all other specimen dimensions. This is the situation we focus on in this work and it allows to assume 'small-scale yielding' conditions to hold, i.e., all inelastic processes are confined to a small region around the crack tip (the

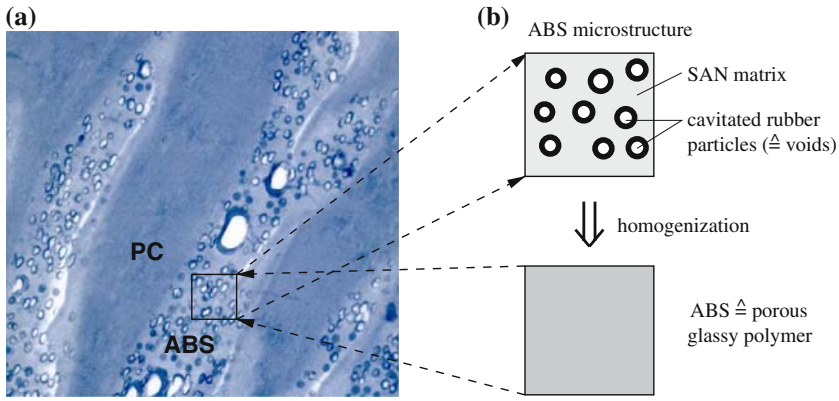

Fig. 1 (**a**) Microstructure of real PC/ABS (Inberg 2001) and (**b**) modeling as a two-phase material of PC and homogenized ABS

so-called 'process zone') outside of which the material behaves linear elastically (Fig. 2). The near crack tip fields then are uniquely controlled by the stress intensity factor K and numerical modeling can be resticted to the K-field dominated region. The computational models in the present work are two-dimensional and plane strain conditions are considered. Mode I loading is imposed in terms of the respective displacements $\boldsymbol{u}$ prescribed as far-field boundary conditions, see e.g., (Lai and Van der Giessen 1997). Inside the process zone the two-phase blend microstructure is explicitly resolved and different morphologies—particulate or lamellar—are considered as sketched in Fig. 2. This type of modeling is, in terms of length scales, the opposite extreme case to that analyzed in (Seelig and Van der Giessen 2002) where PC/ABS blends subjected to uniform overall loading were investigated. Finite element discretizations of the numerically analyzed K-field dominated region and the encompassed process zone (for the case of a particulate morphology) are shown in Fig. 3. Due to the mode I symmetry only half of the problem needs to be modeled. According to Fig. 3b the crack tip radius in the model is about two times the ABS particle diameter; via this interrelation and a typical ABS particle diameter of about 5μm (Greco 1996) an absolute value of about $r_{\text{tip}} = 10\mu$m can be assigned to the crack tip radius in the computational model.

The finite strain inelastic constitutive models for the individual phases (PC and ABS) in the process zone are presented in Sects. 3.1 and 3.2. Outside the process zone where no plasticity takes place effective elastic constants obtained from homogenizing the PC/ABS could be used. However, micromechanical analyses by Seelig (2004) have shown that for the range of composition considered here the variation of the effective stiffness of PC/ABS around that of neat PC is not more than about $\pm 10\%$. In view of other, more severe simplifications this variation as well as a possible elastic anisotropy in case of lamellar morphologies are neglected in the present study and material parameters for neat PC are used for the material outside the process zone.

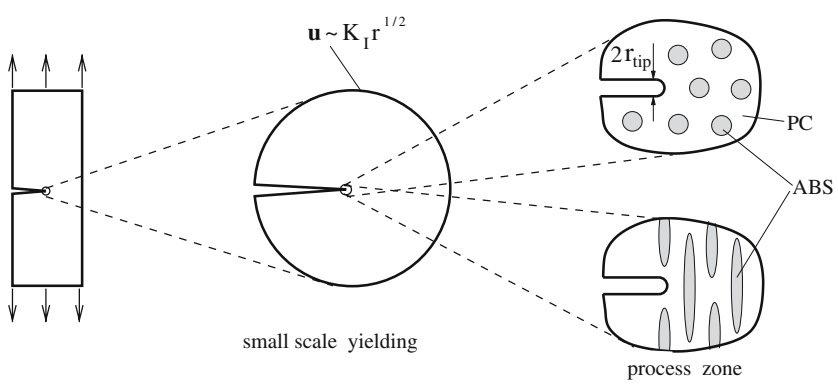

Fig. 2 Crack tip modeling in PC/ABS blends under small-scale yielding conditions

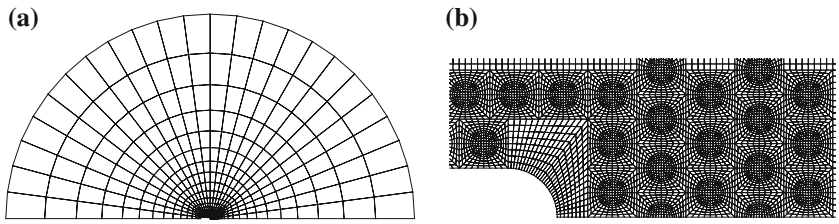

Fig. 3 Finite element meshes of entire crack tip region (**a**) and process zone (**b**)

2.3 Cohesive zone modeling of failure

The fracture model sketched in Fig. 2 in conjunction with the constitutive models to be described in Sects. 3.1 and 3.2 will be evaluated in Sect. 4.1 with regard to effects of the blend microstructure on the situation (e.g., local fields) at a stationary crack tip. In order to analyze effects on the fracture toughness, however, one needs to account for a fracture process. For the simulation of mode I crack propagation in Sect. 4.2, the mechanical model is supplemented by a cohesive surface along the symmetry axis inside the process zone as sketched in Fig. 4. The cohesive surface is endowed with different properties representing failure in the alternating PC and ABS regions along the crack path, as will be discussed in Sects. 3.3 and 3.4. Attention will be restricted to the case of equal volume fractions (50/50) of PC and ABS where the real microstructure often displays a lamellar morphology (see Fig. 1) as sketched in Fig. 4.

3 Constitutive modeling

3.1 Homogeneous glassy polymers

Constitutive models for the large strain visco-plastic deformation behavior of amorphous glassy polymers are quite well established in the literature; see e.g., (Smit et al. 1999), (Gearing and Anand 2004). In the present work we employ the model originally developed by Boyce et al. (1988) in the slightly modified version given in (Wu and Van der Giessen 1996). Here it is adopted to represent the behavior of the PC matrix on the blend level as well as that of the SAN matrix in the ABS model (Sect. 3.2), though with different sets of material parameters as listed in Table 1.

The theory makes use of the standard additive decomposition of the rate of deformation tensor into its elastic and plastic parts: $\boldsymbol{D} = \boldsymbol{D}^{\mathrm{e}} + \boldsymbol{D}^{\mathrm{p}}$. Visco-elastic effects prior to yield are of minor importance in the present study and are neglected. The small strain elastic response is governed by Hooke's law written in rate form as

$$\boldsymbol{D}^{\mathrm{e}} = \boldsymbol{\mathcal{L}}^{-1} \overset{\nabla}{\boldsymbol{\sigma}} \tag{1}$$

where $\overset{\nabla}{\boldsymbol{\sigma}}$ is the Jaumann rate of the Cauchy stress and $\boldsymbol{\mathcal{L}}$ is the standard fourth-order isotropic elasticity tensor. The isochoric visco-plastic strain rate

$$\boldsymbol{D}^{\mathrm{p}} = \frac{\dot{\gamma}^{\mathrm{p}}}{\sqrt{2}\tau}\bar{\boldsymbol{\sigma}}' \tag{2}$$

is specified in terms of the equivalent plastic shear strain rate $\dot{\gamma}^{\mathrm{p}} = \sqrt{\boldsymbol{D}^{\mathrm{p}} \cdot \boldsymbol{D}^{\mathrm{p}}}$ and the deviatoric driving stress $\bar{\boldsymbol{\sigma}}'$ normalized by the equivalent driving shear stress $\tau = \sqrt{\frac{1}{2}\bar{\boldsymbol{\sigma}}' \cdot \bar{\boldsymbol{\sigma}}'}$. The latter serves to determine $\dot{\gamma}^{\mathrm{p}}$ via the visco-plastic constitutive equation

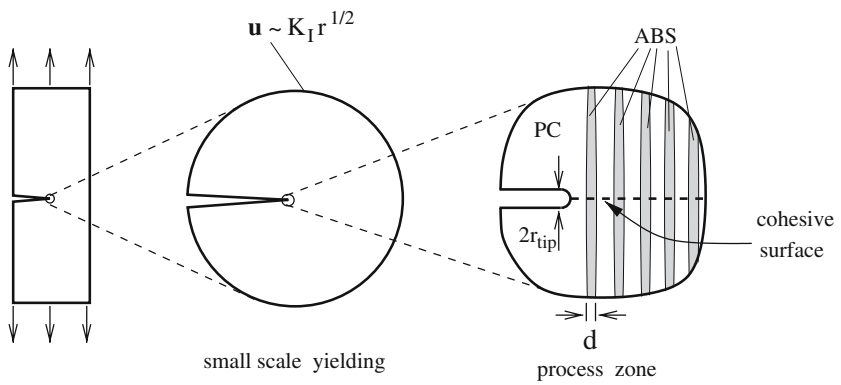

Fig. 4 Modeling mode I crack propagation in co-continuous PC/ABS (50/50) blend

Table 1 Material parameters used for PC and SAN at room temperature in the present work

	E/s_0	ν	s_s/s_0	As_0/θ	h/s_0	α	$\lambda_{\max}$	C^R/s_0	s_0 (MPa)	$\dot{\gamma}_0$ (sec^{-1})
PC	9.4	0.3	0.79	79.2	5.15	0.08	2.5	0.059	97	$2 \cdot 10^{15}$
SAN	12.5	0.38	0.79	52.2	12.6	0.25	3.5	0.033	120	$1.06 \cdot 10^{8}$

$$\dot{\gamma}^{\mathrm{p}} = \dot{\gamma}_0 \exp\left[-\frac{A\tilde{s}}{\theta}\left(1 - \left(\frac{\tau}{\tilde{s}}\right)^{5/6}\right)\right] \tag{3}$$

where $\dot{\gamma}_0$ and A are material parameters, and θ is the absolute temperature which is constant in the present analysis. The shear resistance $\tilde{s}$ in (3) is taken to evolve with plastic strain according to

$$\tilde{s}(\gamma^{\mathrm{p}}) = s_s + (s_0 - s_s)\exp\left(-h\gamma^{\mathrm{p}}/s_s\right) + \alpha p \tag{4}$$

from the initial, athermal yield strength s_0 to a saturation value s_s in order to phenomenologically describe the intrinsic softening of the glassy polymer (Boyce et al. 1988). Furthermore, (4) incorporates the dependence of yield on the pressure $p = -\frac{1}{3}\mathrm{tr}\boldsymbol{\sigma}$ via the constant pre-factor α. This pressure dependence is due to a changing molecular mobility and not associated with plastic dilatancy of the bulk material, $\mathrm{tr}\boldsymbol{D}^{\mathrm{p}} = 0$. From (2) and the definition of τ it follows that the plastic dissipation rate per unit volume of the material is given by $\bar{\boldsymbol{\sigma}}' \cdot \boldsymbol{D}^{\mathrm{p}} = \sqrt{2}\tau\dot{\gamma}^{\mathrm{p}}$.

The progressive hardening of a glassy polymer after yield due to stretching and alignment of the molecular network is described by the back stress tensor $\boldsymbol{b}$ incorporated in the driving stress tensor $\bar{\boldsymbol{\sigma}}' = \boldsymbol{\sigma}' - \boldsymbol{b}$. Drawing on the analogy with cross-linked rubber (Arruda and Boyce 1993) the principal components of the back stress tensor are specified in terms of principal stretches. The back stress model involves two additional material parameters: the initial hardening modulus C_R and the limit stretch of the molecular chains $\lambda_{\max}$ at which the network responds with an infinite stiffness and no further yielding is possible. Full details of the constitutive model may be found in (Wu and Van der Giessen 1996) along with a convenient numerical integration scheme.

The response of the constitutive model for glassy polymers under plane strain tension and at constant strain rate is illustrated in Fig. 5. It is based on the sets of material data for PC and SAN listed in Table 1 which are adopted from (Boyce et al. 1988) and (Steenbrink and Van der Giessen 1999). The model well captures characteristic features of the behavior of glassy polymers such as the intrinsic softening upon yield and the progressive rehardening. It should be mentioned that the values for Young's modulus in Table 1 are smaller that those typically given in the literature because here, by neglecting the nonlinear deformation regime prior to yield, they represent the secant moduli corresponding to the yield stress and yield strain of the materials.

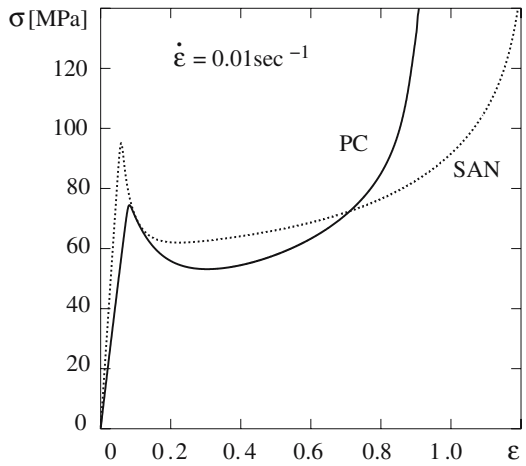

Fig. 5 Plane strain tension response of PC and SAN in terms of true stress vs. logarithmic strain at constant strain rate and room temperature, computed from data in Table 1

3.2 Homogenized ABS model

Experimental (e.g. Ramaswamy and Lesser 2002) as well as numerical (Pijnenburg et al. 2005) studies have shown that caviation of the rubber particles in ABS close to a crack tip takes place in an early stage of loading and at stress states well below the yield (or crazing) stress. Once cavitated, the stiffness of these particles can be neglected compared to that of the surrounding matrix and therefore the rubber particles in the present work are treated as voids from the beginning on. The overall behavior of ABS can then be approximated by that of porous SAN. The SAN itself, being the thermoplastic matrix phase in ABS, is described by the constitutive model given in the previous section. The isotropic

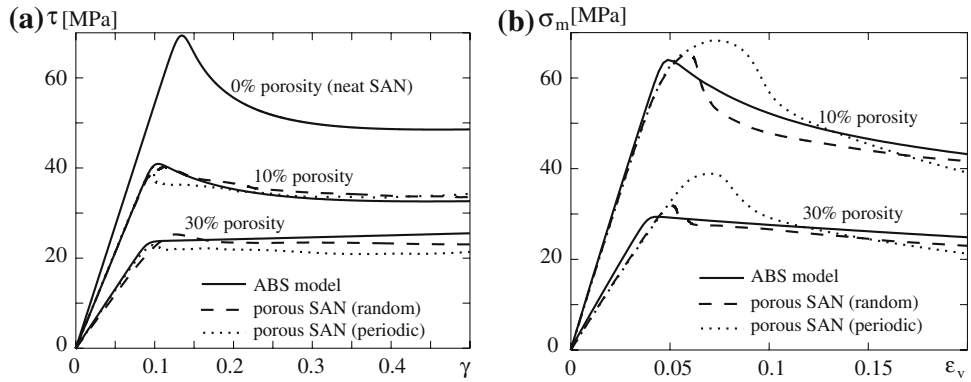

Fig. 6 Overall response of RVE and homogenized ABS model to simple shear (**a**) and equi-biaxial strain (**b**)

elasticity tensor for the porous material is now given in terms of effective elastic constants $E^*(f)$, $\nu^*(f)$ depending on the porosity f. Respective expressions can be found, e.g., in (Pijnenburg and Van der Giessen 2001). With the initial value f_0 representing the rubber content in ABS, the porosity may evolve in the course of deformation according to $\dot{f} = (1-f)D^{\mathrm{p}}_{kk}$ due to void growth in the plastically incompressible SAN matrix. Hence, macroscopic yielding of the porous material will involve plastic dilatancy under hydrostatic stress. For this, we adopt the phenomenological macroscopic yield function

$$\Phi \equiv \frac{1}{2}\bar{\boldsymbol{\sigma}}' \cdot \bar{\boldsymbol{\sigma}}' + a f_0^b \sigma_m^2 - [(1-f)\tau c]^2 \tag{5}$$

which exhibits a quadratic dependence on the deviatoric and hydrostatic stress. The parameters a and b express the influence of hydrostatic (mean) stress σ_m and are fitted to values of $a \approx 1$ and $b \approx 0.7$ from calculations with a representative volume element of voided SAN. The parameter c is a function of f_0 determined from micromechanical considerations (Seelig and Van der Giessen 2002) as $c \approx (1+\sqrt{f_0})^{-1}$. The equivalent driving stress τ in the SAN matrix phase due to the stress $\boldsymbol{\sigma}$ acting on the porous material is determined from the condition $\Phi = 0$. The plastic strain rate is determined via the (normality) flow rule

$$\boldsymbol{D}^{\mathrm{p}} = \Lambda \frac{\partial \Phi}{\partial \bar{\boldsymbol{\sigma}}} \tag{6}$$

where the multiplier Λ is computed from the condition that the plastic work rate per unit deformed volume of the porous material equals that in the matrix:

$$\bar{\boldsymbol{\sigma}} \cdot \boldsymbol{D}^{\mathrm{p}} = (1-f)\sqrt{2}\tau\dot{\gamma}^{\mathrm{p}} \,. \tag{7}$$

With the equivalent driving stress τ solved from (5), the equivalent plastic strain rate $\dot{\gamma}^{\mathrm{p}}$ obtained from (3) now represents the 'effective' visco-plastic behavior of the entire matrix phase. Due to the highly heterogeneous plastic flow in a porous glassy polymer the intrinsic softening of the matrix is evened out in the overall response as supported by large scale simulations by Smit et al. (1999). To incorporate this effect in the homogenized model, intrinsic softening is taken to decrease with increasing porosity. Full details on this modeling of ABS as a porous glassy polymer may be found in (Seelig and Van der Giessen, 2002).

Figure 6 shows the response of the homogenized ABS model in comparison to the overall response of unit cell computations of a representative volume element with a SAN matrix and different void arrangements, under macroscopic simple shear and equi-biaxial strain. For values of the porosity in the relevant range, the homogenized ABS model captures the elastic stiffness, the yield point, as well as the post-yield behavior of a porous glassy polymer to an acceptable degree of accuracy. Also shown in Fig. 6a is the response of neat SAN, i.e. ABS with 0% rubber content (porosity). The decrease of the elastic stiffness and yield strength of ABS with increasing rubber content featured by the present model is in good qualitative agreement with experimental findings (Ishikawa 1995). It should be mentioned that the volumetric expansion enforced by highly triaxial loading (Fig. 6b) leads to an overall softening response due to void growth in the post-yield regime.

3.3 Crazing in PC

Failure of neat glassy polymers (here PC) typically proceeds by the formation and propagation of a craze in which the polymeric material is drawn into numerous fibrils (of a few nanometers thickness) of highly stretched and oriented molecules (e.g., Narisawa and Yee 1993; Haward and Young 1997; Estevez et al. 2000). These fibrils connect the two craze–bulk interfaces and are able to transfer stress until they rupture and the craze locally turns into a crack, typically at a critical craze width (depending on the material) of the order of a micron or below. Representing the effect of stress-carrying fibrils between the separating craze-bulk interfaces in the course of craze widening by a rate-dependent traction–separation law, Tijssens et al. (2000) have developed a cohesive surface model for crazing. This model was subsequently applied by Estevez et al. (2000, 2005) to investigate the competition between bulk plasticity (shear yielding) and crazing in homogeneous glassy polymers; it is also employed in the present work to model failure by crazing in the PC regions of PC/ABS blends. The crazing cohesive model recognizes three stages: craze initiation, craze widening and craze breakdown, which will now be presented briefly.

Craze initiation in glassy polymers is mainly governed by hydrostatic stress and a number of different criteria may be found in the literature (e.g., Kinloch and Young 1983; Narisawa and Yee 1993). Based on experiments, Sternstein and coworkers proposed a criterion which states that craze initiation takes place when the maximum principal stress T_n reaches a critical value σ_n^{cr} which is a decreasing function of hydrostatic stress σ_m (Estevez et al. 2000):

$$T_n = \sigma_n^{cr}(\sigma_m) \equiv \sigma_m - \frac{A}{2} s_0 + \frac{B}{6}\frac{s_0^2}{\sigma_m} \,. \tag{8}$$

Here, s_0 is the athermal yield strength of the bulk polymer (Table 1). Through the direction of maximum principal stress the above criterion also determines the craze orientation which, however, is fixed in the present study. The relation (8) is shown in Fig. 7a along with the influence of the parameter B and displays the aforementioned strong influence of hydrostatic stress on craze initiation. Since the criterion (8) appears to be only meaningful in the range where the critical tensile stress is a decreasing function of hydrostatic stress, it is beyond that range continued with constant values indicated by the dotted part of the curves in Fig. 7a.

The relation between the traction T_n normal to the craze and the separation Δ_n of the craze-bulk interfaces is written in the following elastic visco-plastic rate form (Tijssens et al. 2000):

$$\dot{T}_n = k_n \left(\dot{\Delta}_n - \dot{\Delta}_n^c \right) . \tag{9}$$

Prior to craze initiation the visco-plastic craze widening rate $\dot{\Delta}_n^c$ vanishes and the elastic stiffness k_n is a large, purely artificial 'penalty' parameter. After initiation k_n reflects the instantaneous elastic stiffness of the craze matter. For craze widening upon initiation, a visco-plastic relation analogous to (3) has been proposed by Tijssens et al. (2000)

$$\dot{\Delta}_n^c = \dot{\Delta}_{0n} \exp\left[-\frac{A_c \sigma_c}{\theta} \left(1 - \frac{T_n}{\sigma_c} \right) \right] \tag{10}$$

where $\dot{\Delta}_{0n}$, A_c and σ_c are material constants and θ is the (here constant) absolute temperature. Hence, craze widening at a constant rate is assumed to take place at a constant stress (e.g. $T_n = \sigma_c$ at $\dot{\Delta}_n^c = \dot{\Delta}_{0n}$). Values for these parameters which cannot be directly related to their bulk counterparts in (3) are fairly unclear, and assuming them to be constant is a severe simplification. The reason for the fundamental difference from the bulk behavior is that complex processes of disentanglement and molecular chain-scission, necessary for the drawing of fibrils, take place in the so-called 'active zone' at the craze-bulk interface (Tijssens et al. 2000; Estevez et al. 2000). These processes locally change the characteristics of the molecular network, e.g. its hardening behavior, and may introduce a rate-dependence by their own. Following heuristic arguments in (Estevez et al. 2000) the values of material parameters given in Table 2 are assumed in the present work.

The typical response of the cohesive law at a constant widening rate is shown in Fig. 7b. Craze initiation here has been assumed to take place at $T_n = 100\,\text{MPa}$ whereas the widening resistance in (10) has a value of $\sigma_c \approx 90\,\text{MPa}$ (Table 2). Since $T_n > \sigma_c$ at craze initiation, the visco-plastic widening rate $\dot{\Delta}_n^c$ computed from (10) initially is very large and via (9) causes the sharp drop of T_n seen in Fig. 7b. Thereby $\dot{\Delta}_n^c$ decreases until it reaches the value of the (here prescribed) total widening rate $\dot{\Delta}_n$, and T_n according to (9) attains a constant value. This plateau value is somewhat lower than σ_c since $\dot{\Delta}_n < \dot{\Delta}_{0n}$ has been chosen here. Finally, when the craze has widened to a critical value $\Delta_n^{c\,cr}$ the cohesive traction T_n is rapidly (stepwise in numerical simulations) decreased to zero to describe breakdown

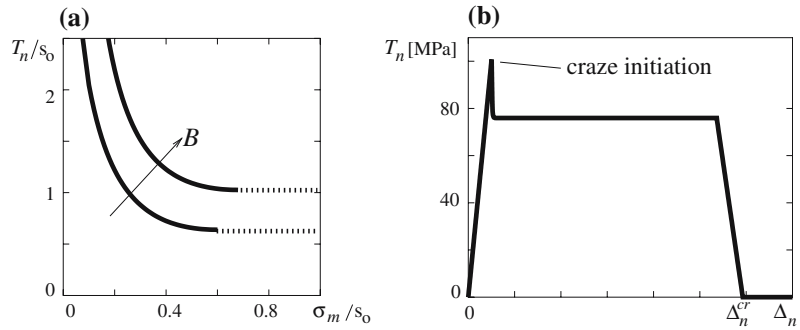

Fig. 7 (**a**) Craze initiation criterion and (**b**) traction-separation law for crazing in PC at a constant widening rate $\dot{\Delta}_n/\Delta_n^{cr} = 10/\mathrm{s}$

Table 2 Material parameters used in cohesive surface model for crazing in PC at room temperature in the present work

A	B	σ_c/s_0	$A_c\sigma_c/\theta$	$\dot{\Delta}_{0n}/\Delta_n^{c\,cr}$ (sec^{-1})	$k_n\Delta_n^{c\,cr}$ (MPa)	$\Delta_n^{c\,cr}/r_{\mathrm{tip}}$
0.7	2.8	0.9	44	10^3	10^3	0.2

of the craze. It has to be noted that the cohesive traction T_n after craze initiation depends on the widening rate $\dot{\Delta}_n$ and therefore the (specific) work of separation, i.e. the area under the curve in Fig. 7b, is in general not constant.

As mentioned in (Haward and Young 1997) crazing is less likely to occur in material that has already undergone plastic deformation because of the stretching of the molecular network. It is therefore assumed here that crazing can only take place if the maximum principal stretch is less than 2, i.e., 80% of the limit stretch $\lambda_{\max}$ of PC according to Table 1. If this value is reached prior to crazing at some point along the cohesive surface, the material there is considered to fail by brittle rupture once it has fully locked and a critical tensile stress of 150 MPa is reached. This strength value, which can be estimated from the molecular structure of PC (Seitz 1993) corresponds to the fully locked regime in Fig. 5. Brittle rupture (at zero length of decohesion) is treated numerically by releasing the traction to zero in a small number of time steps.

3.4 Failure of ABS

In contrast to neat glassy polymers (e.g., PC above) where failure takes place by a single craze it appears rather unclear how to set up a cohesive zone model for fracture in ABS. The reason is that failure of ABS is typically preceded by the formation and coalescence of multiple crazes between the rubber particles. Since multiple crazing often also contributes to the inelastic bulk deformation of ABS it is hardly possible to uniquely separate the bulk behavior from the (cohesive) fracture process zone behavior. For simplicity, a cohesive zone model of the same general structure as that for PC is adopted here, yet with properties corresponding to the bulk deformation behavior of ABS. Obviously, appropriate parameter values are fairly unclear and a number of assumptions and estimates from heuristic considerations therefore have to be made. The cohesive strength σ_c entering the rate-dependent traction-separation law analogous to (10) is taken to scale with the area fraction of the stress-carrying ligament between voids (times the yield strength s_s of SAN, Table 1). For the 2D case of cylindrical voids to which also the porous plasticity model for bulk ABS has been fitted (Sect. 3.2) this means that $\sigma_c(f_0) \sim 1 - \sqrt{f_0}$. Initiation of the separation process is assumed to take place at a critical value $T_n^{cr}(f_0)$ of the normal traction on the cohesive surface which depends on the porosity in a similar fashion as $\sigma_c(f_0)$. Since the deformation behavior of ABS according to Sect. 3.2 as well as the cohesive law for separation display a plateau-like behavior (see Figs. 6 and 8) these values have to be picked carefully to guarantee a continuous transition from mere bulk deformation to separation. The values used in the simulations are listed in Table 3. A reasonable estimate for the critical separation $\Delta_n^{c\,cr}$ at which the cohesive traction T_n decreases to zero appears to be of the order of the rubber particle size. Whether or not it should be taken to depend on the rubber content is not clear; here it is assumed constant and half the value chosen for PC,

Table 3 Values used in cohesive zone model for ABS

f_0	T_n^{cr} (MPa)	σ_c (MPa)
0.1	65	70
0.15	60	65
0.25	45	55
0.4	30	45
0.5	20	35

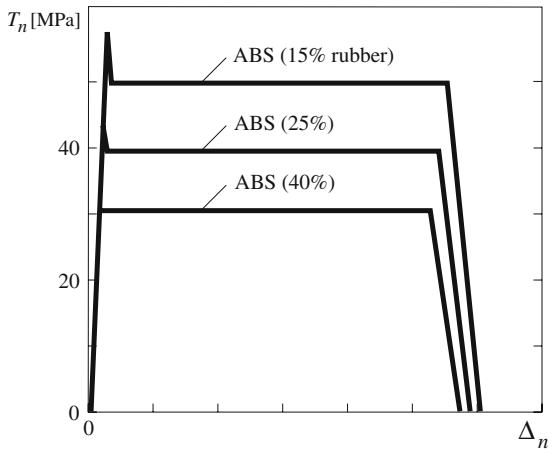

Fig. 8 Traction-separation law for failure of ABS at a constant widening rate $\dot{\Delta}_n/\Delta_n^{cr} = 10/\mathrm{s}$

i.e. $\Delta_n^{c\,cr}(\mathrm{ABS}) = 0.5\Delta_n^{c\,cr}(\mathrm{PC})$. All other parameters in the cohesive relation (10), governing essentially the dependence on rate and temperature, are for simplicity taken equal to those in the cohesive zone model for PC. The response of the cohesive zone model for ABS at a constant separation rate is shown in Fig. 8 for different values of the rubber content. Due to the rate dependence the traction levels at initiation and during separation need not be the same as indicated by the 'overshoot' at initiation.

As an alternative to the above model, one could fully map the transition to failure into the bulk deformation behavior and simply release (at zero length of decohesion, numerically in several steps) the tractions on the cohesive surface once a critical strain has been attained in the adjacent bulk material. In the present blend model, however, this approach would cause a conflict with the cohesive zone model of the neighboring PC which has a finite length of decohesion.

4 Results

In the following the fracture mechanical models sketched in Figs. 2 and 4 are evaluated numerically. Loading is prescribed in terms of the applied stress intensity factor K_I which is normalized as $\bar{K} = K_I/s_0\sqrt{r_{\mathrm{tip}}}$ with the yield strength $s_0 = 97\,\mathrm{MPa}$ of PC (Table 1) and the crack tip radius r_{tip}. A constant loading rate $\dot{\bar{K}} = 1/\mathrm{sec}$ is chosen in all simulations. With $r_{\mathrm{tip}} \approx 10\mu\mathrm{m}$ this corresponds to $\dot{K} \approx 0.3\,\mathrm{MPa}\sqrt{\mathrm{m}}/\mathrm{sec}$ which is well in the range where isothermal conditions (assumed in the present work) are likely to prevail as has been analyzed by Estevez et al. (2005).

4.1 Crack tip fields at a stationary crack tip

The toughness of a material arises from energy dissipation in the various mechanisms but in laboratory tests they cannot be aportioned. The emphasis in the present section is on the effect of blend microstructure on energy dissipation prior to fracture and the underlying development of a plastic zone. The propensity of fracture initiation is monitored in terms of local stresses responsible for triggering crazing. Different morphologies—particulate and lamellar—as they occur in real PC/ABS blends are considered.

4.1.1 Effect of morphology

The superior fracture toughness of PC/ABS blends compared to neat PC in the presence of sharp notches or pre-cracks is commonly ascribed to the occurrence of massive plastic deformation enabled by the ABS and to the suppression of crazing in the PC (e.g., Lee et al. 1992; Greco et al. 1994; Inberg 2001). The latter is a consequence of a relief of hydrostatic stress caused by the dilation of the ABS. To illustrate how these mechanisms act in the framework of the present model, Fig. 9 shows the distribution of equivalent plastic strain rate $\dot{\gamma}^{\mathrm{p}}$ (left) and hydrostatic stress σ_m (right) in the vicinity of a crack tip in neat PC (top) and two PC/ABS blends each containing 30% ABS with 10% rubber (center and bottom). In the center of Fig. 9 a morphology with dispersed ABS particles is considered as it is found for real blends with 30% ABS. The 'lamellar' morphology of elongated regions of PC and ABS (bottom) typically prevails in the range of approximately equal contents of both phases (e.g. Greco et al. 1994; Inberg 2001),

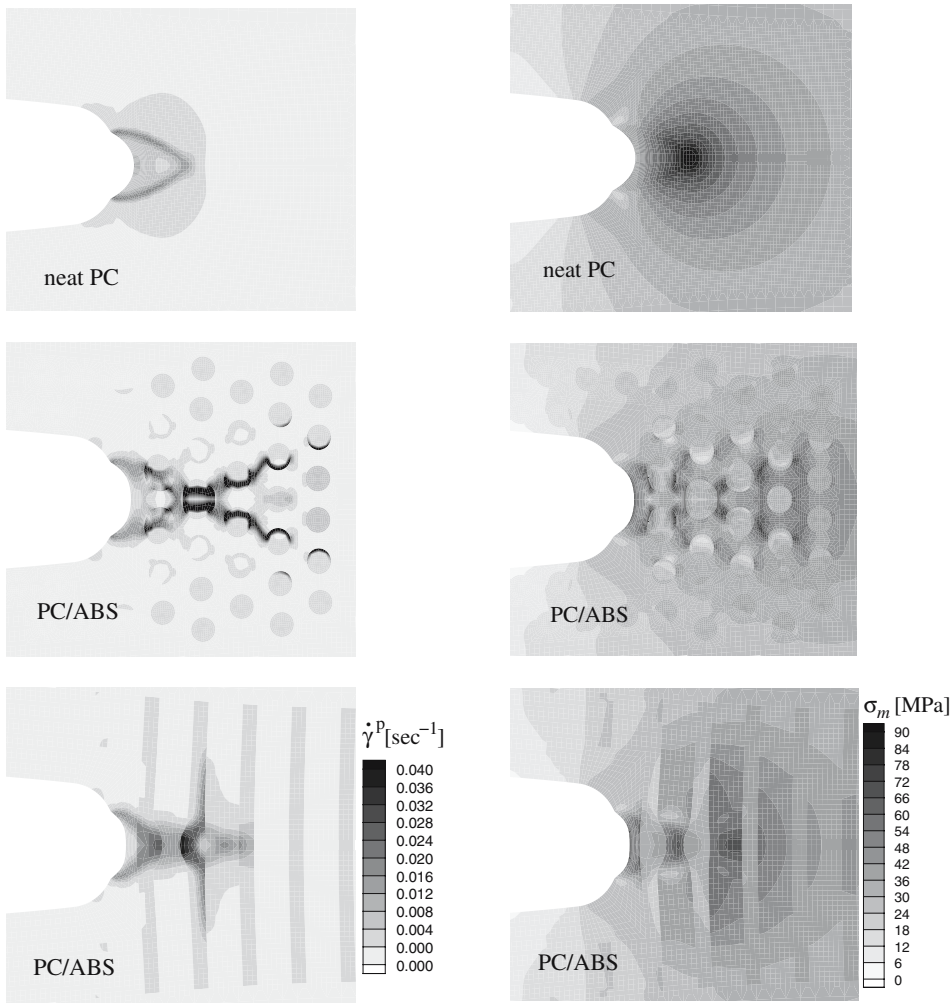

Fig. 9 Equivalent plastic strain rate (left) and hydrostatic stress (right) at stationary crack tip in neat PC (top) and PC/ABS blends (30% ABS, 10% rubber in ABS) of particulate (center) and lamellar (bottom) morphology at normalized stress intensity factor $\bar{K} = 2.25$

but is considered here anyway in order to gain some insight in the qualitative sensitivity to morphology.

As already mentioned earlier, plastic deformation at a notch under plane strain conditions in neat PC takes place by the formation of a pair of shear bands which intersect at some distance ahead of the notch (Narisawa and Yee 1993; Lai and Van der Giessen 1997; Estevez et al. 2000; Gearing and Anand 2004). Close to this intersection a concentration of hydrostatic stress appears (Fig. 9 top) which can lead to the initiation of a single craze as a precursor of brittle failure. Obviously, plastic flow and hydrostatic stress are more delocalized in the presence of ABS (center and bottom of Fig. 9). In case of the particulate morphology, yielding is seen to take place inside the ABS particles as well as in the PC matrix. The particles close to the crack tip display pronounced volumetric expansion. In the microstructure with ABS layers perpendicular to the crack (Fig. 9 bottom), plastic flow in both phases spreads successively along the layers. For both morphologies the plastic zone in the PC/ABS blends is significantly larger than in neat PC. At the same time, the values

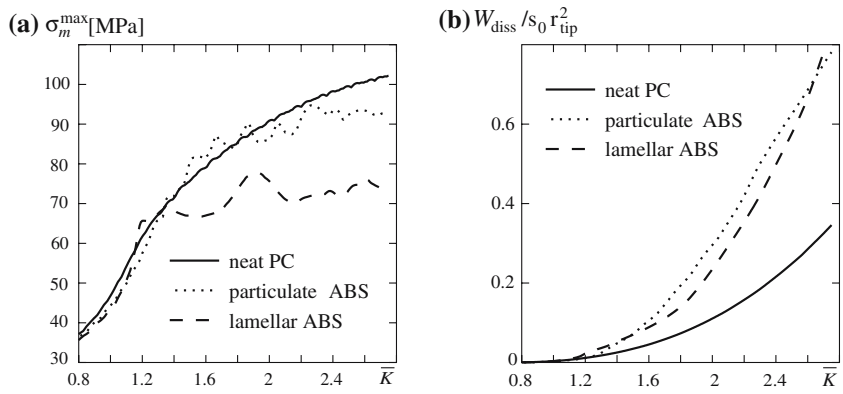

Fig. 10 Effect of morphology of PC/ABS blends on (**a**) peak hydrostatic stress in the PC phase and (**b**) energy dissipation (per unit thickness); both blends contain 30% ABS with 10% rubber

of hydrostatic stress in the blends are lower and less concentrated than in neat PC. Multiple stress peaks are visible in the PC matrix, especially in case of the particulate microstructure, and if these would initiate crazing it would take place more distributed than in neat PC. Both, the energy dissipation associated with plastic flow and the reduction and delocalization of hydrostatic stress are indicative of a higher toughness of the PC/ABS blends; some more quantitative results are presented below.

The amount of volumetric expansion of the ABS enabled by its porosity (rubber) can qualitatively be seen from the distribution of hydrostatic stress. For both morphologies, σ_m in the ABS phase at locations further away from the crack tip is higher than in the surrounding PC matrix because of the higher bulk modulus of ABS at low (initial) porosity. Closer to the crack tip the opposite holds, since the capacity of ABS to carry hydrostatic stress there has strongly decreased due to the increase of the porosity.

The peak value of hydrostatic stress, $\sigma_m^{\max}$, (being critical for craze initiation) found in the PC matrix throughout the process zone and the dissipated work $W_{\rm diss} = \int_0^t \int_V \bar{\boldsymbol{\sigma}} \cdot \boldsymbol{D}^{\rm p} {\rm d}V\,{\rm d}t$ can be considered as toughening indicators and are traced in the course of loading. In correspondence to Fig. 9, the effect of different morphologies of PC/ABS blends on $\sigma_m^{\max}$ and on $W_{\rm diss}$ (per unit thickness in the present plane strain problem and normalized by $s_0 r_{\rm tip}^2$) is depicted in Fig. 10. To smooth out local effects resulting only from the particular arrangement of the ABS close to the crack tip, averaging over three different realizations of the microstructure is performed for each of the two morphologies. Also shown in Fig. 10 is the response of neat PC. Obviously, local peak values of hydrostatic stress in the PC are more affected by the blend morphology than the (global) energy dissipation. The latter is nearly the same for both PC/ABS blends and, as expected, significantly higher than for neat PC. In the particulate microstructure the hydrostatic stress still attains values of about 90 MPa which according to the literature (e.g. Kinloch and Young 1983; Narisawa and Yee 1993) may cause craze initiation in PC. However, peak hydrostatic stresses then prevail at several locations between the ABS particles (Fig. 9, center) and eventual failure would probably occur less localized than in neat PC. The values of hydrostatic stress in case of the lamellar morphology suggest that crazing is suppressed. One has to bear in mind, however, that local stress concentrations in the PC induced by possible localized failure mechanisms inside the ABS (see discussion in Sect. 5) are not accounted for in the present model since it treats ABS as a homogeneous porous medium.

4.1.2 Effect of rubber content in ABS

The importance of plastic dilatancy of the ABS for toughening is illustrated by comparing the above results to the behavior of a PC/SAN blend, i.e., 0% rubber, where both phases are plastically incompressible. Figure 11 shows the distribution of plastic strain rate $\dot{\gamma}^{\rm p}$ (a) and hydrostatic stress σ_m (b) for the same 30% particle morphology as in the center of Fig. 9. It is clearly seen that the localization of plastic flow in shear bands and the concentration of hydrostatic stress in one strong peak found in neat PC (Fig. 9, top) is only slightly disturbed by the presence of SAN. Enlargement of the plastic zone and delocalization of hydrostatic stress accomplished by the ABS (Fig. 9, center and bottom) can—at

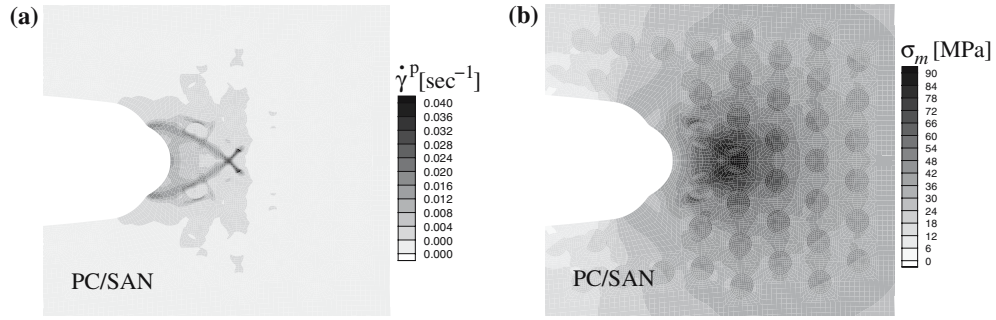

Fig. 11 Distribution of equivalent plastic strain rate (**a**) and hydrostatic stress (**b**) in PC/SAN blend (i.e., 0% rubber in ABS) with 30% SAN particles at $\bar{K} = 2.25$

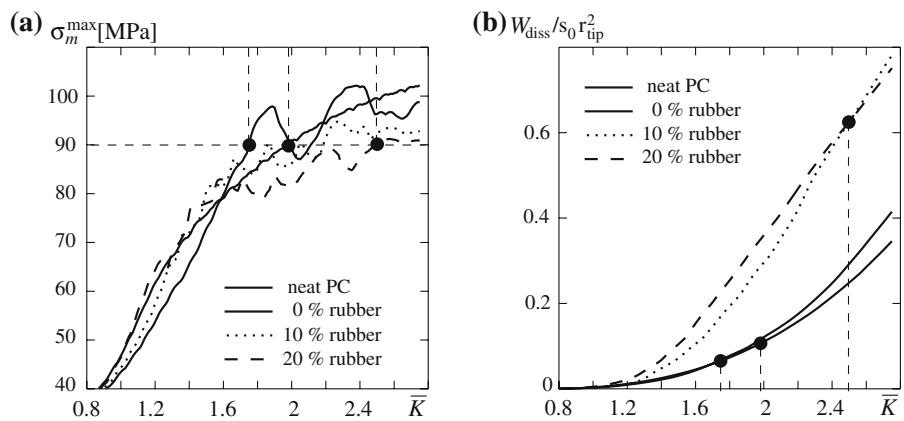

Fig. 12 Effect of rubber content in ABS on (**a**) peak hydrostatic stress in the PC phase and (**b**) energy dissipation (per unit thickness); 30% ABS particles. The •'s mark for each case the initiation of crazing when this is assumed to occur when the hydrostatic stress reaches a value of 90 MPa

least according to the present model—not be achieved by blending PC with SAN.

The rubber content in ABS is reported to be a parameter of utmost importance for toughening in real PC/ABS blends (Greco 1996). Its effect in the framework of the present model is depicted in Fig. 12. The microstructure considered here consists of 30% dispersed particles (see center of Fig. 9). Again the response of neat PC is shown for comparison. Peak values of hydrostatic stress found in the PC matrix decrease with increasing rubber content in ABS (10% and 20%) while for the extreme case of a PC/SAN blend (0% rubber, as shown in Fig. 11) they clearly exceed those prevailing in neat PC. Energy dissipation in the PC/SAN blend is very low and comparable to that in neat PC whereas it is significantly enhanced by the presence of some amount of rubber (porosity) in the ABS (Fig. 12b).

One way to crudely interpret the present results with regard to the fracture initiation toughness is to look at the onset of failure which can be associated with craze initiation in the PC; according to Narisawa and Yee (1993) this occurs at a critical hydrostatic stress of about 90 MPa. The intersection of the corresponding horizontal line with the different curves in Fig. 12a yields the critical loading stages in terms of $\bar{K}$ at which the individual materials would fail (indicated by •). The related amounts of dissipated energy can then be obtained from Fig. 12b. Comparing the values for PC/ABS with 20% rubber, neat PC and PC/SAN leads to the ratio PC/ABS : PC : PC/SAN $\approx$ 10 : 2 : 1. Though not directly comparable with the situation considered here because of the different loading conditions, experimental results by Kurauchi and Ohta (1984) should be mentioned who found a similar ordering in the impact fracture energy with values for PC/ABS about ten times higher than those for PC/SAN.

As an alternative to the peak hydrostatic stress σ_m^{max} considered in the present work as an indicator for craze

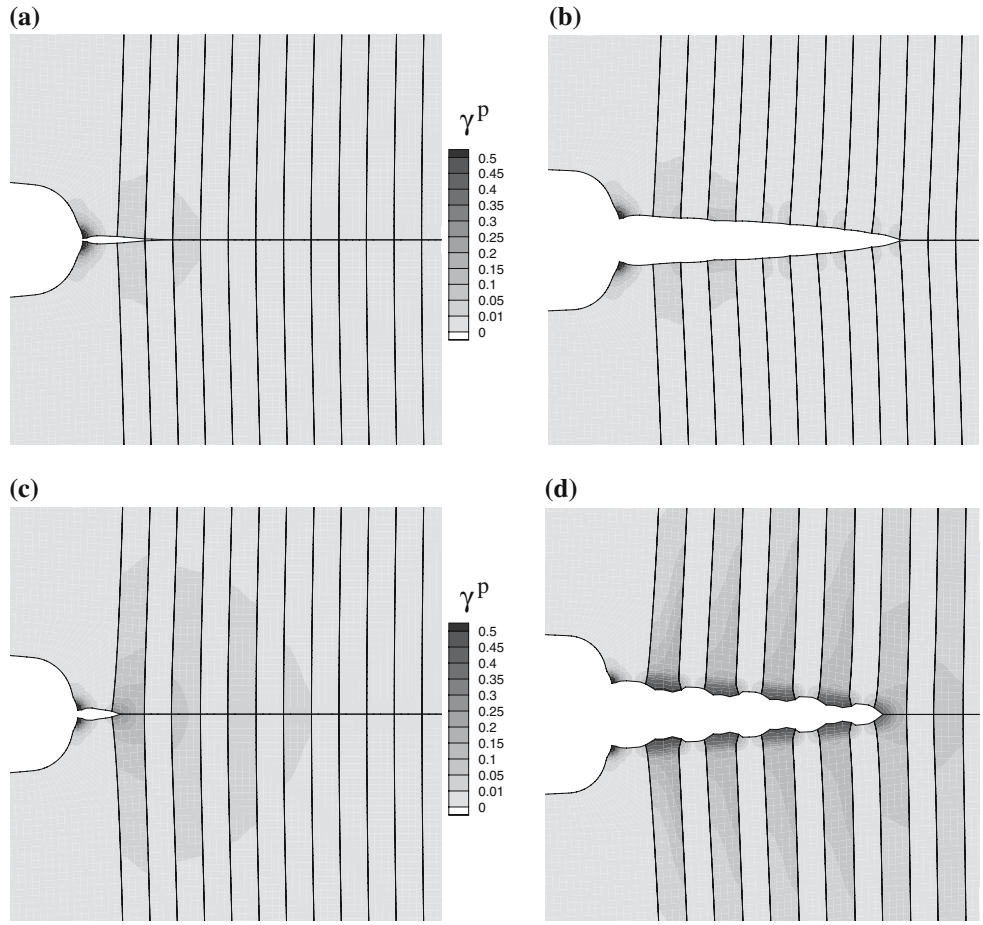

Fig. 13 Crack propagation and plastic zone evolution in PC/ABS (50/50) blends with 15% rubber (**a**, **b**) and 40% rubber (**c**, **d**) in the ABS

initiation, one may evaluate Sternstein's $\sigma_n^{cr}(\sigma_m)$ criterion (8) which varies with $\bar{K}$ in a similar way as $\sigma_m^{\max}$ (Seelig et al. 2001). Common to both criteria is the decreasing slope of the variation of the critical stress with increasing $\bar{K}$ which makes it difficult to trace the onset of crazing. It therefore might be interesting to look instead at strain-based craze initiation criteria as are discussed e.g., in (Kinloch and Young 1983); yet much less data are available in terms of craze initiation strain than in terms of stress.

4.2 Crack growth

The model employed in the previous section is now extended to allow for crack propagation as sketched in Fig. 4. Here we consider only the case of a co-continuous morphology with equal volume fractions of PC and ABS, and focus on the effect of the rubber content in ABS. The blend microstructure with layers of both phases perpendicular to the initial crack is resolved inside the process zone where plastic flow and crack propagation are expected to take place. The elastic (far-field) region outside the process zone is, for simplicity again, described using the isotropic elastic constants of neat PC. The error made by ignoring the proper (here anisotropic) overall elastic behavior of PC/ABS is believed to be small compared to uncertainties in modeling deformation and failure in the process zone. The same constitutive models for PC and ABS as in the previous sections are employed here, i.e., ABS is again described as a porous plastic medium with the porosity reflecting the rubber content. Failure and crack propagation are considered only along the symmetry axis

of the problem where a cohesive surface is introduced (see Fig. 4) with alternating properties for the PC and ABS layers as specified in Sects. 3.3 and 3.4. Since the morphology and the ABS content are fixed in the present model, the rubber content (porosity) in the ABS is the only remaining "free" microstructural parameter with its effect on the fracture process to be investigated. Blends with a rubber content in the ABS varying between 15% and 50% are being considered. As in the previous section, loading is imposed via far-field boundary conditions determined by the normalized mode I stress intensity factor $\bar{K} = K_I/s_0\sqrt{r_{\text{tip}}}$. The lamellar morphology of real (50/50) PC/ABS blends typically shows a layer thickness of approximately 2–5μm (Inberg 2001). From the relative length scales visible in Fig. 13 this means that the crack tip radius r_{tip} in the computational model is on the order of 10μm (as in Sect. 4.1, see also Sect. 2).

Figure 13 shows snap-shots of the evolving plastic zone, in terms of the distribution of accumulated plastic strain, as the crack propagates. The figures on the left (a, c) refer to the onset of crack propagation, i.e., the first occurrence of cohesive zone failure ('breakdown') while the figures on the right (b, d) show the situation at an amount of crack advance of about $6r_{\text{tip}}$. The performance of the two blends, with rubber contents of 15% and 40%, differs significantly in the amount of plastic deformation. In the case of the low rubber content (Fig. 13a and b) the lateral extension of the plastic zone decreases with increasing crack length. In contrast, the plastic zone in the blend with a large rubber content (Fig. 13c and d) is larger after some amount of crack growth (right) than at crack initiation (left). The plastic zone size tends to a stationary width in the ABS layers which is significantly larger than the initial crack tip radius. Massive plastic deformation of PC and ABS can be seen along the fracture surface (Fig. 13d).

The effect of ABS rubber content on the fracture toughness is shown in Fig. 14 in terms of so-called *R*-curves. Blends with a relatively low rubber content (here 15% and 25%) fail in a brittle manner, i.e., the crack resistance does not increase with crack propagation after initiation—in accordance with the lack of a pronounced plastic zone seen in the 15% rubber blend in Fig. 13a and b. In contrast, the build-up of a large plastic zone (see Fig. 13c and d) in blends with a higher rubber content in the ABS (here 40% and 50%) leads to an increase of the fracture toughness in the course of crack growth. Neat PC, as discussed before and included in Fig. 14 for reference, displays brittle failure; yet, its toughness is higher than the initiation toughness of the PC/ABS blends considered here. Hence, the initiation of fracture taking place somewhere ahead of the notch root (Fig. 13a and c) in the present blend model is promoted by the presence of the ABS layers. Crack initiation starts earlier, i.e., at a lower load level, in case of blends with a larger amount of rubber (softer ABS) which, however, subsequently display an *R*-curve behavior.

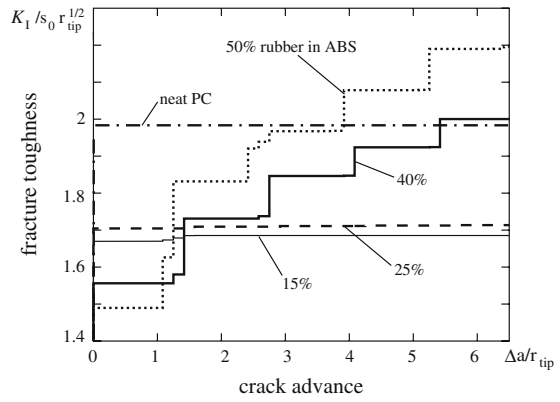

Fig. 14 Crack resistance curves for neat PC and co-continuous PC/ABS (50/50) blends with different rubber content in ABS

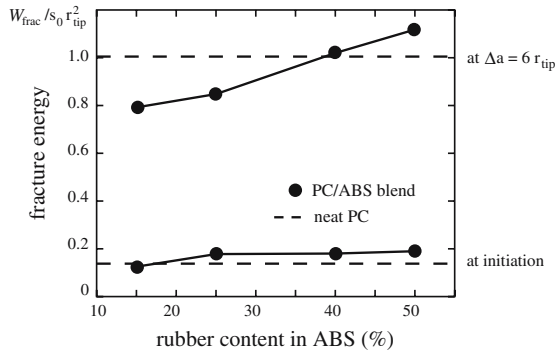

Fig. 15 Fracture energy (per unit thickness) vs. rubber content in ABS at two stages of crack propagation

The total fracture energy, i.e., the work dissipated in the course of the fracture process, consists of the work of separation (expended in the cohesive zone) plus the dissipation in the bulk (plastic zone): $W_{\text{frac}} = W_{\text{sep}}$ (cohes. zone) $+ W_{\text{diss}}$ (bulk). In fracture testing of polymers (e.g., IZOD), W_{frac} is often considered as a global measure of toughness. Figure 15 shows, for

two stages of the fracture process corresponding to the snap-shots in Fig. 13, the fracture energy as a function of the rubber content in ABS computed from the present blend model. Obviously, the rubber content in ABS has a stronger effect on the energy absorption during fracture than at crack initiation. This agrees with the observation made from Fig. 13 that the amount of rubber in ABS determines, at least in the framework of the present model, whether massive energy dissipation in a growing plastic zone takes place or not. A 'synergistic effect' in terms of an optimal rubber content, as reported in part of the experimental literature (see Introduction), however, cannot be detected from the present simulations.

5 Discussion and conclusions

The present study is concerned with the fracture processes in amorphous thermoplastic PC/ABS blends. In order to investigate micromechanisms and microstructural effects in these materials, the situation at a crack tip has been modeled by resolving the blend microstructure around the crack tip and by accounting for failure of the different phases of the heterogeneous material. Thereby a number of assumptions have been made and a critical assessment of these assumptions with respect to the overall response predicted in terms of the fracture toughness seems to be pertinent.

Results so far have been presented in terms of normalized stress intensity factors and normalized work of fracture. Absolute values of these quantities are obtained if an absolute value is assigned to the crack tip radius r_{tip}. The crack tip radius in the present computational model is fixed by its size relative to the ABS particles and layers (Figs. 3b and 13). With the latter known from micrographs, we obtain a typical value of $r_{\text{tip}} \approx 10\,\mu$m, as mentioned in Sect. 2.2. According to Fig. 14 and with $s_0 \approx 100$ MPa this yields a fracture initiation toughness (K_{Ic}) of about 0.63 MPa$\sqrt{\text{m}}$ for neat PC and about 0.5 MPa$\sqrt{\text{m}}$ for PC/ABS. These values are significantly lower than experimental data reported in the literature, i.e. $K_{Ic} \approx 2$ MPa$\sqrt{\text{m}}$ for neat PC (e.g., Kinloch and Young 1983) and $K_{Ic} \approx 1.5$ MPa$\sqrt{\text{m}}$ for PC/ABS (Seidler and Grellmann 1993), but are consistent with the tendency that the initiation toughness of PC/ABS is roughly 75% below that of neat PC. The origin of the quantitative difference, however, is not obvious. One possible, and in fact likely, reason may be that the crack tip radius of about 10 μm in the present model is smaller than that in the fracture tests underlying the above experimental data (Inberg and Gaymans 2002). Modeling a larger crack tip with respect to the microstructure (particle size), however, would enormously increase the numerical expense due to the discretization of the correspondingly larger process zone. Another reason might be that the critical stress values in the local failure initiation criteria have been chosen too small in the present study. A more thorough investigation of these issues will be subject of future work.

The results presented in Sect. 4.2 show an increasing fracture toughness of PC/ABS with increasing rubber content. So, an issue to be commented on is the synergistic effect, i.e., the optimal toughness for some intermediate range of composition, observed in some experimental studies but not reproduced in the simulations. A simple explanation is that the situations for which such a synergistic effect is reported are not captured by the present simulations. In (Greco et al. 1994) a synergistic effect was observed only for blends with particulate ABS (about 30%) whereas crack growth simulations here are performed only for a lamellar morphology. The synergistic effect reported by Inberg (2001) for a lamellar morphology was ascribed to massive delamination of the PC and ABS layers. Incorporation of this additional failure mechanism, e.g., by cohesive surfaces, would introduce additional material parameters for which reliable data are presently not available.

A further difference between experiments and simulations is due to the loading rates. While the present simulations are performed at a low rate of loading and under isothermal conditions the experiments by Greco et al. (1994) and by Inberg (2001) showing synergistic effects were done at rather high loading rates. Under these conditions the significant temperature rise due to adiabatic heating (Inberg 2001) may play an important role and affect the measured toughness. Modeling high rate fracture processes in future analyses requires to take these effects into account as done for homogeneous glassy polymers in (Estevez et al. 2005).

A benefit of micromechanical models is that they yield information about quantities not accessible to measurements, such as, for instance, the amount of energy dissipated in the individual phases of a heterogeneous material such as PC/ABS. A common view in the experimental literature is that toughening in PC/ABS is

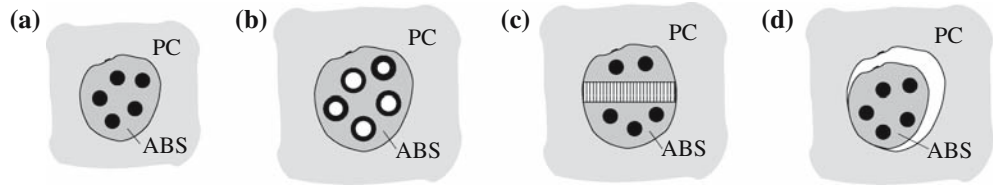

Fig. 16 Sketch of undeformed PC/ABS blend (**a**) and mechanisms causing a relief of hydrostatic stress: (**b**) rubber particle cavitation and void growth in ABS, (**c**) crazing in ABS, (**d**) debonding along interface

mainly due to plastic (shear) yielding in the PC enabled by the volumetric expansion and the relief of hydrostatic stress accomplished by the ABS. The present work is based on the assumption that void growth from cavitated rubber particles inside the ABS is the dominant mechanism for this. Probably as a consequence of this assumption, simulations predict a large portion of the total energy dissipation to take place in the ABS by plastic deformation of its matrix (SAN). However, as sketched in Fig. 16, other mechanisms such as crazing inside the ABS or interface debonding may likewise accomplish the volumetric expansion necessary for yielding of neighboring PC regions under overall triaxial loading conditions. Indeed, each of the three mechanisms sketched in Fig. 16b–d is found in real ABS and, for instance, interface debonding has been suggested to play an important role in toughening of co-continuous PC/ABS blends (Inberg 2001). Thus, more micromechanical studies are needed (or at least helpful) to better understand the competition and the conditions for the predominance of the different micromechanisms; this is a subject of ongoing work (Seelig and Van der Giessen 2006).

References

Arruda EM, Boyce MC (1993) A three-dimensional constitutive model for the large stretch behavior of rubber elastic materials. J Mech Phys Solids 41:389–412

Balakrishnan S, Neelakantan NR (1998) Mechanical properties of blends of polycarbonate with unmodified and maleic anhydrite grafted ABS. Polymer Int 45:347–352

Boyce MC, Parks DM, Argon AS (1988) Large inelastic deformation of glassy polymers. Mech Mater 7:15–33

Bucknall CB (1977) Toughened plastics. Applied Science, London

Danielsson M, Parks DM, Boyce M (2002) Three-dimensional micromechanical modeling of voided polymeric materials. J Mech Phys Solids 50:351–379

Estevez R, Tijssens MGA, Van der Giessen E (2000) Modeling the competition between shear yielding and crazing in glassy polymers. J Mech Phys Solids 48:2582–2617

Estevez R, Van der Giessen E (2005) Modeling and computational analysis of fracture of glassy polymers. Adv Polymer Sci 188:195–234

Estevez R, Basu S, Van der Giessen E (2005) Analysis of temperature effects near mode I cracks in glassy polymers. Int J Frac 132:249–273

Gearing BP, Anand L (2004) Notch-sensitive fracture of polycarbonate. Int J Solids Struc 41:827–845

Greco R, Astarita MF, Dong L, Sorrentino A (1994) Polycarbonate/ABS blends: processability, thermal properties, and mechanical and impact behavior. Adv Polymer Technol 13(4):259–274

Greco R (1996) Polycarbonate toughening by ABS. In: Martuscelli E, Musto P, Ragosta G (eds) Advanced routes for polymer toughening. Elsevier, pp 469–526

Haward RN, Young RJ (1997) The physics of glassy polymers. Chapman & Hall

Inberg JPF (2001) Fracture of polycarbonate/ABS blends. PhD Thesis, University of Twente, Enschede, The Netherlands

Inberg JPF, Gaymans RJ (2002) Polycarbonate and co-continuous polycarbonate/ABS blends: influence of notch radius. Polymer 43:4197–4205

Ishikawa M (1995) Stability of plastic deformation and toughness of polycarbonate blended with poly (acrylonitrile-butadiene-styrene) copolymer. Polymer 36:2203–2210

Ishikawa M, Chiba I (1990) Toughening mechanisms of blends of poly(acrylonitrile-butadiene-styrene) copolymer and BPA polycarbonate. Polymer 31:1232–1238

Kinloch AJ, Young RJ (1983) Fracture behaviour of polymers. Applied Science Publishers

Kurauchi T, Ohta T (1984) Energy absorption in blends of polycarbonate with ABS and SAN. J Mater Sci 19:1699–1709

Lai J, Van der Giessen E (1997) A numerical study of crack-tip plasticity in glassy polymers. Mech Mater 25:183–197

Lee M-P, Hiltner A, Baer E (1992) Fractography of injection moulded polycarbonate acrylonitrile-butadiene-styrene terpolymer blends. Polymer Eng Sci 32(13):909–919

Meijer HEH, Govaert LE (2003) Multi-scale analysis of mechanical properties of polymer systems. Macromol Chem Phys 204:274–288

Narisawa I, Yee AF (1993) Crazing and fracture of polymers. In: Thomas EL (ed) Structure and properies of polymers; Material Science and Technology, A Comprehensive Treatment, Vol 12. VCH, pp 698–765

Pijnenburg KGW, Van der Giessen E (2001) Macroscopic yield in cavitated polymer blends. Int J Solids Struc 38:3575–3598

Pijnenburg KGW, Seelig Th, Van der Giessen E (2005) Successively refined models for crack tip plasticity in polymer blends. Eur J Mech, A/Solids 24:740–756

Ramaswamy S, Lesser AJ (2002) Microscopic damage and macroscopic yield in acrylonitrile-butadiene styrene (ABS) resins tested under multi-axial stress states. Polymer 43:3743–3752

Seelig Th (2004) On micromechanical modeling of toughening mechanisms and failure in amorphous thermoplastic polymer blends. Habilitation Thesis, TU Darmstadt, Germany

Seelig Th, Van der Giessen E, Gross D (2001) Numerical simulation of crack tip fields and toughening mechanisms in ternary polymer blends. In: Ravi-Chandar K, et al. (eds) Advances in fracture research, ICF10, on CD-ROM

Seelig Th, Van der Giessen E (2002) Localized plastic deformation in ternary polymer blends. Int J Solids Struc 39:3505–3522

Seelig Th, Van der Giessen E (2006) Modeling the interaction of crazing and matrix plasticity in rubber-toughened polymers. In: Meijer HEH (ed) Proc Int Conference on Deformation, Yield and Fracture of Polymers. Kerkrade, pp 275–278

Seidler S, Grellmann W (1993) Fracture behavior and morphology of PC/ABS blends. J Mater Sci 28:4078–4084

Seitz JT (1993) The estimation of mechanical properties of polymers from molecular structure. J Appl Pol Sci 49:1331–1351

Smit RJM, Brekelmans WAM, Meijer HEH (1999) Prediction of the large-strain mechanical response of heterogeneous polymer systems: local and global deformation behavior of a representative volume element of voided polycarbonate. J Mech Phys Solids 47:201–221

Socrate S, Boyce MC (2000) Micromechanics of toughened polycarbonate. J Mech Phys Solids 48:233–273

Steenbrink AC, Van der Giessen E (1999) On cavitation, post-cavitation and yield in amorphous polymer-rubber blends. J Mech Phys Solids 47:843–876

Tijssens MGA,Van der Giessen E, Sluys LJ (2000) Modeling of crazing using a cohesive surface methodolgy. Mech Mater 32:19–35

Wu PD, Van der Giessen E (1996) Computational aspects of localized deformations in amorphous glassy polymers. Eur J Mech A/Solids 15:799–823